Asian Journal of Chemistry; Vol. 36, No. 7 (2024), 1470-1482

ASIAN JOURNAL OF CHEMISTRY

https://doi.org/10.14233/ajchem.2024.31286

Removal of Methylene Blue by Activated Carbon from Jackfruit: Kinetic, Isothermal Evaluation and Optimization Using by Response Surface Methodology

BICH NGOC HOANG[1,*], THI CAM QUYEN NGO[1], LAM VAN TAN[2], THI KIM NGAN TRAN[1], THI TUU TRAN[1], SY CHI PHUNG[1] and ANH DUC PHUNG[1]

[1]Institute of Applied Technology and Sustainable Development, Nguyen Tat Thanh University, Ho Chi Minh City 700000, Vietnam
[2]Ben Tre Department of Science and Technology, Ben Tre Province, Vietnam

*Corresponding author: E-mail: bichhn@ntt.edu.vn

Received: 24 January 2024; *Accepted*: 5 April 2024; *Published online*: 29 June 2024; AJC-21663

Activated carbons derived from the byproducts of jackfruit processing, specifically the skin (peel) and pulp, were prepared using the chemical assisted microwave irradiation method. The structural and physical properties were evaluated based on the results of scanning electron microscope, X-ray diffraction patterns, Fourier-transform infrared spectroscopy, Brunauer–Emmett–Teller theory analysis. The results have shown that activated carbon from jackfruit skin and activated carbon from jackfruit pulp have a honeycomb shape with a surface area of 268 $m^2 g^{-1}$ and 309 $m^2 g^{-1}$, respectively. Both samples showed the presence of specific functional groups such as C=C, C=O, O–H and C–H. It can be seen that the material structure was semi-crystalline and clearly shown in the 2θ value ranges which are 2θ = 20-35º and 40-45º. Specifically, 2θ = 20-35º represents the structural characteristics of the carbon or graphite lattice. Factors that influence the removal of methylene blue that have been evaluated which include adsorption time, solution pH, ambient temperature, activated carbon dosage, dye concentration and optimization by the response surface methodology model. The parameters for the adsorption process are optimized from the response surface methodology model with activated carbon from jackfruit pulp (pH 8.97, concentration of 50.5 mg L^{-1}, dosage of 0.57 g L^{-1}, time 120 min, temperature 30 ºC, the adsorption capacity of 90.82 mg g^{-1}, adsorption efficiency 100%) and activated carbon from Jackfruit skin (pH 8.61, concentration 52 mg L^{-1}, dosage 0.57 g L^{-1}, time 120 min, temperature 30 ºC, adsorption capacity 94.04 mg g^{-1}, adsorption efficiency 100%), respectively. The adsorption process shows that activated carbon from jackfruit pulp (ACJP) follows the pseudo-second order and Langmuir model and activated carbon from jackfruit skin (peel) (ACJS) follows the model of Bangham and Langmuir. The adsorption process is predicted with many mechanisms, including chemical interactions, multilayer adsorption and diffusion. The materials showed application potential as the reusability was three times.

Keywords: Activated carbon, Methylene blue, Response surface methodology, Jackfruit, Kinetic, Isothermal.

INTRODUCTION

Jackfruit with scientific name *Artocarpus heterophyllus*, family: Moraceae, Genus: Artocarpus, this is a fruit plant common in Brazil and Southeast Asia [1,2]. The authors used data from the International Center for Agriculture and Biological Sciences (CABI) to present the properties of jackfruit [3]. The jackfruit tree is a complex, oval-shaped fruit and bears fruit after 3 years of age. Jackfruit is a fruit with a fleshy, sweet, aromatic taste, contains a lot of sugar and has high nutritional value and is a good medicine in traditional medicine [4,5]. Products from jackfruit have been researched and widely applied in the world such as jackfruit juice, dried jackfruit, jackfruit ice cream, jackfruit seed powder and snacks from jackfruit [6-11]. Therefore, jackfruit is widely grown in Vietnam and applied in the food industry. Large byproduct amounts from jackfruit were discharged into the environment, although jackfruit trees bring many economic benefits. During processing, the by-products of jackfruit (*e.g.* skin and pulp) were discard as organic wastes. jackfruit skin contains about 27.75% of cellulose, 7.52% of pectin, 6.27% of protein and 4% of starch [12]. The jackfruit pulp contains carbohydrates (20.5%), crude protein (10.6%) and crude fiber (15.9%) [13]. Even, they were caused many environmental problems such as toxic gases, water pollution and breeding grounds for most pathogenic microorganisms [14]. To contribute to environmental protection, researchers

have aimed to turn the skin and pulp of jackfruit into activated carbon thanks to the thick and porous structure of the shell. Ngan Tran *et al*. [15] showed the ability to turn jackfruit by-products into activated carbon. Jackfruit peel activated carbon was synthetic with activators such as phosphoric acid, nickel(II) hydroxide, potassium hydroxide, sodium hydroxide and sulfuric acid [16-20]. It can be seen that NaOH is a potential activator for a large surface area [21]. The material has been synthesized by heating with microwave-assisted and different activators. Among the activated carbon synthesis methods, microwave-assisted synthesis has several advantages such as reducing heating time, energy and cost. The use of sodium hydroxide activator and microwave-assisted method were considered for implementation in this study.

Dyes are frequently present in water and contribute to water pollution, as they are extensively used in several sectors including textile, paper, cosmetics, food and toys [22]. The demand for dyes is increasing, the textile industry alone uses about 10,000 tons/year [23]. In textile dyeing wastewater, many kinds of pigments such as malachite green, methylene blue, remazol brilliant blue-R, coomassie violet, Congo red and crystal violet [15,24-26]. Reactive dyes are used for more than 45% of textile products worldwide [22]. In addition, the dye properties can pose a major threat to human health such as toxicity, non-biodegradation and complex structure. The presence of toxic and non-biodegradable methylene blue dye can hinder the penetration of sunlight into the aquatic environment, affecting the photosynthesis of aquatic organisms and causing dissolved oxygen levels to decrease, leading to the degradation of aquatic systems [27,28]. Moreover, it also has adverse effects on human health and environmental damage [29,30].

Converting jackfruit peels to activated carbon would reduce waste disposal costs, provide an inexpensive raw material for commercial activated carbon and help increase its economic value. In this study, jackfruit skin (peel) and pulp were collected as activated carbon raw materials. The materials were synthesized by heating with microwave-assisted method with NaOH activators and using response surface methodology to optimization the removal process of methylene blue in the solution.

EXPERIMENTAL

Methylene blue ($C_{16}H_{18}ClN_3S$) MW: 319.85 g mol^{-1} has a maximum wavelength 664 nm was acquisition from Himedia Laboratories Pvt., Ltd. [31-33]. Sodium hydroxide (NaOH) and hydrochloric acid (HCl) were acquisition from XILONG (Xilong Scientific Co., Ltd). Ethanol absolute (C_2H_5OH) was procured from CHEMSOL, Vietnam.

Preparation of activated carbon: Jackfruit skin (JS) and pulp (JP) were collected from Thu Duc agricultural wholesale market at Ho Chi Minh City, Vietnam. The JS and JP were cut (1 cm × 1 cm in size) and washed thoroughly with water to remove the impurity. The raw materials were dried at 100 ºC for 24 h and pulverized before activation [34]. Raw material was activated by chemical method with the activator being NaOH as described earlier [35]. A total of 50 g of raw materials were impregnated with NaOH at 1:1 (w/w) ratio for 2 h, followed by drying for 24 h at 100 ºC. The microwave-irradiation technique was employed at 600 W to carbonize the material for 2 min. After activation, the activated carbon was washed to remove excess NaOH with 1 M HCl and distilled water at room temperature until it attain a constant pH. Finally, activated carbon from jackfruit skin (ACJS) and activated carbon from jackfruit pulp (ACJP) were dried for 24 h at 110 ºC and stored in a desiccator for subsequent experiments.

Characterization: The morphology of the activated carbons were measured using a scanning electron microscope (SEM) S4800, Japan. The surface functional groups were identified by using the Nicolet 6700 spectrometer (FTIR) in the range of 4000-400 cm^{-1} and using KBr as pellet. The X-ray diffraction (XRD) patterns were scanned at a scan rate of 2º min^{-1} (2θ) with Cu*K*α radiation (1.5406 Å) using a Siemens D5000 Diffractometer. The surface area was analyzed using Brunauer–Emmett–Teller theory (BET) through nitrogen adsorption/desorption with 1 g/cm^3 degas 150 ºC in 12 h by Micromeritics 2020 volume analyzer. Organic dye content in the water sample was measured using a Shimadzu 1601 PC UV-VIS spectrophotometer.

Adsorption process: The adsorption experiments were assessed in a similar manner as described earlier [36]. Some changes were adjusted as follows: dosage of activated carbon varies from 0.05 to 2 g L^{-1}, concentration of methylene blue varies from 0 to 200 mg L^{-1}, time range from 0 min to 330 min, temperature at 30-60 ºC, pH from pH 2-10. Samples were shaken with a thermal incubation shaker at 200 rpm in an Erlenmeyer flask. The dye solutions before and after adsorption were analyzed at 664 nm using UV-Vis spectrometer (Thermo-Fisher Scientific, USA). Eqn. 1 is used to calculate the dye adsorption capacity (Q_e):

$$Q_e = \frac{C_o - C_e}{W \cdot V} \quad (1)$$

where C_e is the dyes concentration after the adsorption process (mg L^{-1}); C_o is the dye concentration before the adsorption process (mg L^{-1}); V is the volume of the dye solution (L); W is the mass of activated carbon (g).

Zeta potential measurement (pHpzc): Determination of pHpzc of materials was done by following the procedure as described earlier [37-39]. Potassium chloride (KCl) (0.1 M) was adjusted the pH index at different pH ranging from 2 to 10 adjusted by HCl (1 mol L^{-1}) and NaOH (0.1 mol L^{-1}). A total of 50 mg of material was added to a flask containing 100 mL of the calibrated KCl solution. The pH values were noted to be initial and final. The final pH was measured and stirred for 48 h at room temperature.

Kinetic and isothermal models of adsorption: In this work, various kinetic models described in the non-linear form include pseudo-first-order (PFO), pseudo-second-order (PSO), Elovich and Bangham models [37-39] were evaluated. The adsorption isotherm model is the basis for suggesting the interaction possibilities between the adsorbent and the dye. Also, provides some insight into the potential adsorption process of the adsorbent. Based on the Langmuir, Freundlich, Temkin and Dubinin-

Radushkevich (D-R) models, the isothermal models were performed and calculated [37-39].

Response surface methodology (RSM): This study optimized activated carbon from jackfruit skin and jackfruit pulp for methylene blue adsorption by response surface method (RSM). Several influencing factors including pH, dosage of adsorbent and initial methylene blue concentration was investigated. There are 5 levels determined to evaluate the model factors including central value (0), low boundary value (-1), high boundary value (+1) and alpha boundary value (±α). Analysis of variance (ANOVA) was used to evaluate the influence of input and output variables along with the correlation between the response function and independent variables and expressed by a quadratic linear regression equation using Design Software Expert software (version 11, State Ease, Minneapolis, USA) [26,40].

Reusability study: The reusability of the activated carbon from jackfruit skin (peel) (ACJS) and activated carbon from jackfruit pulp (ACJP) samples was investigated by weighing and adsorbing under the best condition of the adsorption process. After adsorption, methylene blue concentration was checked by UV-VIS spectrophotometer. Reusable material was soaked with acetone solvent to completely eliminate methylene blue dye. After washing, the material was dried at 70 ºC for 24 h to dry completely. The process was conducted until the adsorption capacity of material decreased by 50% relative to its initial adsorption capability.

RESULTS AND DISCUSSION

To evaluate the handling ability of hazardous substances, the physico-chemical properties, including surface area, surface morphology, pore size or the functional groups present on the surface of the activated carbon materials were specifically analyzed. The surface of the activated carbon was analyzed through SEM images and the results are shown in Fig. 1. It can be seen that the structure of the raw material has large blocks formed with flat surfaces and large pores. Activated carbon was synthesized by the microwave method, which showed the formation of dense voids with the carbon broken into small and coarse particles. The use of microwave in the synthesis process had possibly contributed to improve the material's surface to create the smaller size pores,which had been proved in the study of the Nayak *et al.* [20].

BET studies: Fig. 2 provides the nitrogen desorption isotherms at –150 ºC where ACJP and ACJS were prepared using NaOH for activation at 600W. Based on the IUPAC classification, the N_2 adsorption isotherms of ACJP and ACJS exhibit type IV behaviour with a type-H4 hysteresis loop. Type IV isotherms indicates the existence of well-developed mesoporous within the structure. However, ACJP and ACJS show similar delayed pattern, which indicates that the sorbent has a neutral structure [41,42]. The results of surface area, pore volume and pore size are shown in Table-1. From the BET measurement, the surface area of the raw material was recorded from 0.8 to 1 $m^2 g^{-1}$. With a rather large particle size (6-12 nm), the volume

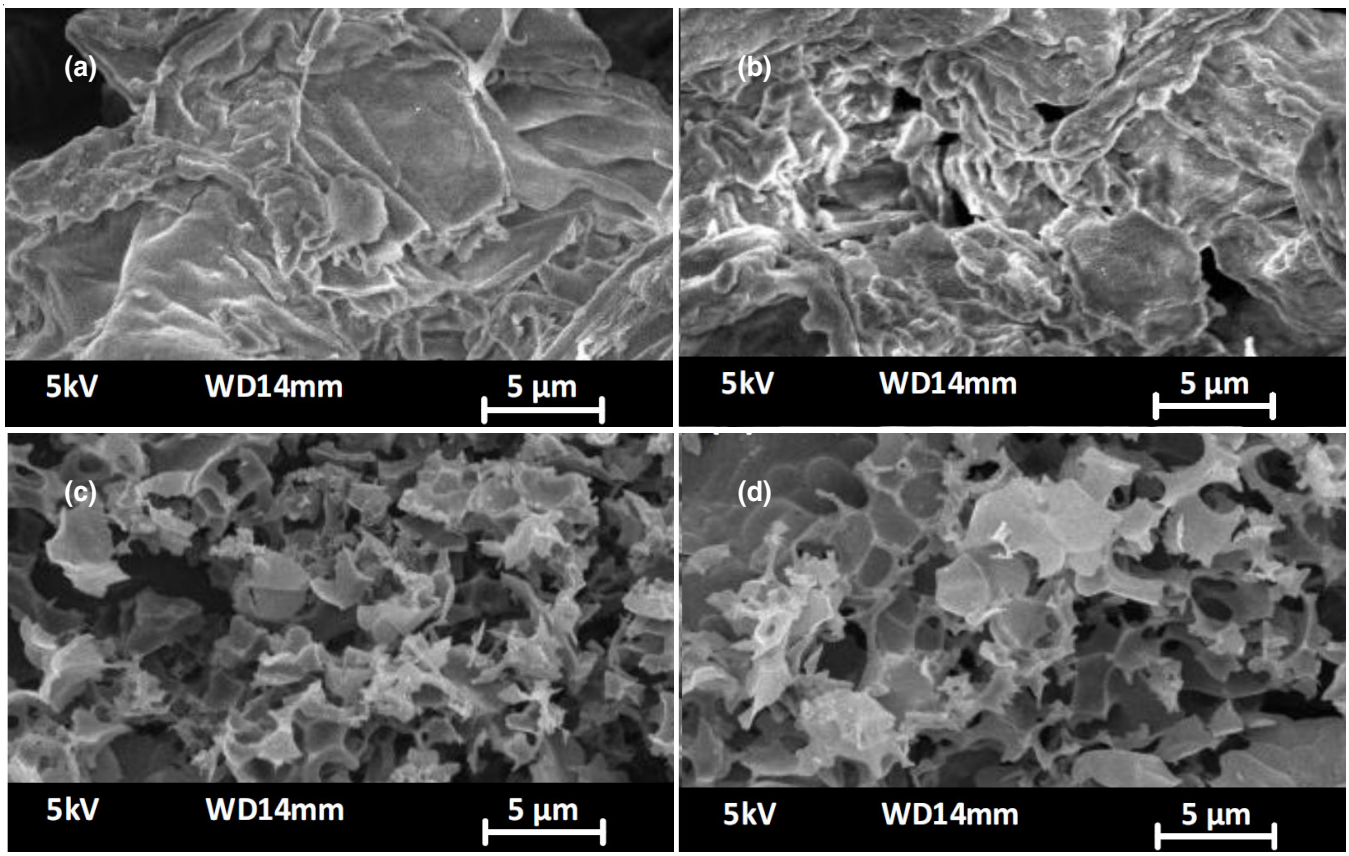

Fig. 1. SEM image of jackfruit pulp (a), jackfruit skin (b), ACJP (c) and ACJS (d)

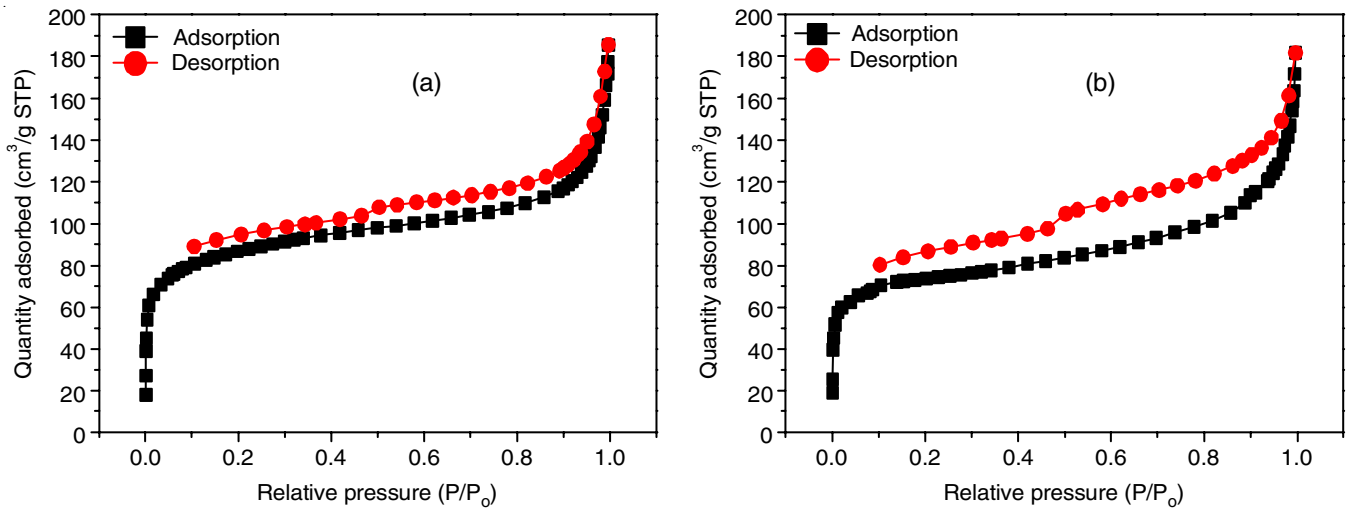

Fig. 2. Nitrogen adsorption–desorption isotherms of ACJS (a) and ACJP (b)

TABLE-1
BET MEASUREMENT RESULTS OF ACJS AND ACJP

Sample	Surface area ($m^2 g^{-1}$)	Pore volumes ($cm^3 g^{-1}$)	Pore size (nm)
JP	1.019	0.003	12.112
JS	0.871	0.001	6.408
ACJP	268.004	0.224	3.674
ACJS	309.261	0.233	3.341

of the pores was found to be in the range from 0.001 to 0.003 $cm^3 g^{-1}$. The results were significantly improved after the KOH activated material with microwave-assisted method. For ACJP, the surface area was increased by more than 200 times compared to the original area. The pore volume was also increased to 0.224 $cm^3 g^{-1}$ and the particle size was about 50% smaller (3.6 nm). Overall, the surface area, pore volume and size were reported to be better for ACJS materials.

FTIR studies: The O–H was recorded at the peak 3700 to 3500 cm^{-1}, which was thought to present for water molecules or hydroxyl groups on the surface of the material (Fig. 3). The N–H group of the amino moiety was found in the range 3500 to 3300 cm^{-1}. The functional groups C–H, C=C, C=O, C–O were also appeared at 2925, 1740, 1604, 1378, 1245, 1070 and 615 cm^{-1}, respectively. The vibration of functional groups has also been demonstrated in previous studies [20,43].

XRD studies: From XRD spectra (Fig. 4), it can be seen that the material structure was semi-crystalline and also clearly shown in the 2θ value ranges 2θ = 20-35º and 2θ = 40-45º. Specifically, 2θ = 20-35º was representing the structural characteristics of the carbon or graphite lattice [20]. This showed that the material can be highly potential for application in adsorption research.

Thermal studies: The thermograms of ACJP and ACJS are shown in Fig. 5. The temperature loss of mass takes place over a temperature range of 50-150 ºC. A small initial decrease in the mass of adsorbent is due to the evaporation of the bound water and moisture in the adsorbent. From this temperature, there is almost no change in sample mass with increasing temperature up to 500 ºC. With 98% remaining sample mass, the sample exhibits a high residual coal content, which indicates

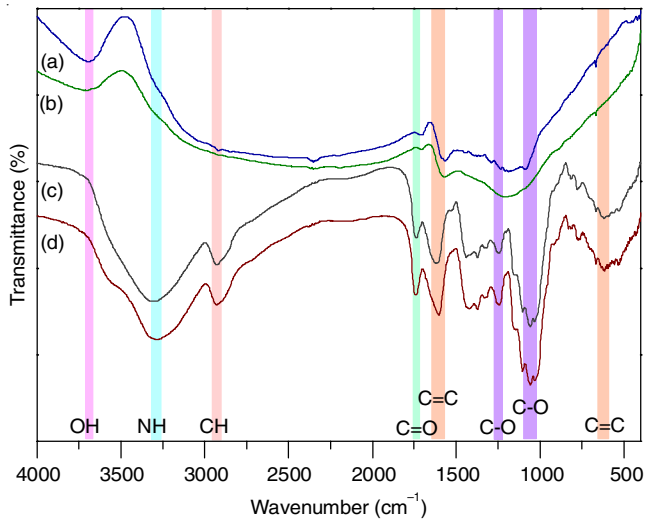

Fig. 3. FTIR spectra of ACJS (a), ACJP (b), jackfruit skin (c) and jackfruit pulp (d)

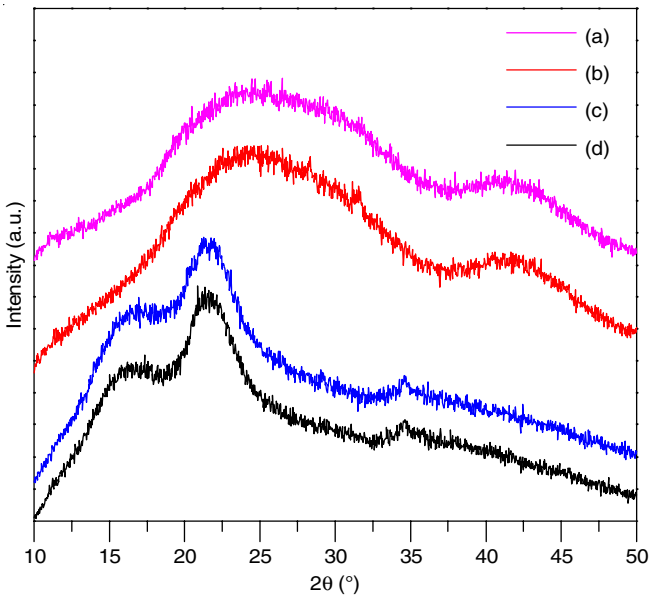

Fig. 4. XRD spectra of ACJS (a), ACJP (b), jackfruit skin (c) and jackfruit pulp (d)

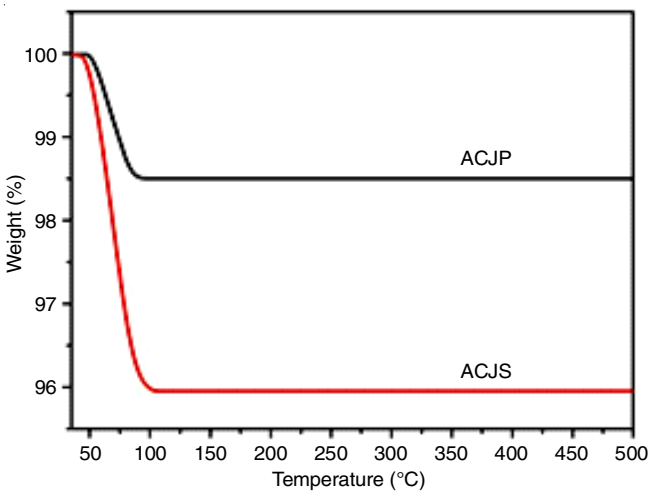

Fig. 5. Thermogravimetric analysis of ACJS and ACJP

that the activation process takes place completely, forming the carbon networks with stable and thermally stable structures [44].

Adsorption studies: The effect of time and temperature during adsorption process are shown in Fig. 6a-b. The results show that the absorption time of ACJP took place quickly from 0-10 min, whereas the adsorption capacity was recorded from 0 to 52 mg g^{-1}. The adsorption process become slow from 52 to 89 mg g^{-1} within next 80 min and the adsorption process almost reached equilibrium at 120 min. The same pattern was also observed in case of ACJS too. The adsorption capacities at the time of equilibration were record as 92 and 80 mg g^{-1} for ACJP and ACJS, respectively. The effect of temperature was evaluated from 30 to 60 ºC, which showed that the adsorption capacity was almost unchanged. It is evident that temperature had no apparent effect on the material adsorption. Thus, the temperature of 30 ºC and 120 min of time were optimized for the further adsorption studies.

Effect of pH: The adsorption capacities at the different pHs (2, 4, 6, 8, 10) are shown in Fig. 7a. For a comprehensive assessment, the pHz value of the material was also evaluated. The pHz values of ACJP and ACJS were found to be 4 and 4.25, respectively. The best pH value in solution was recorded

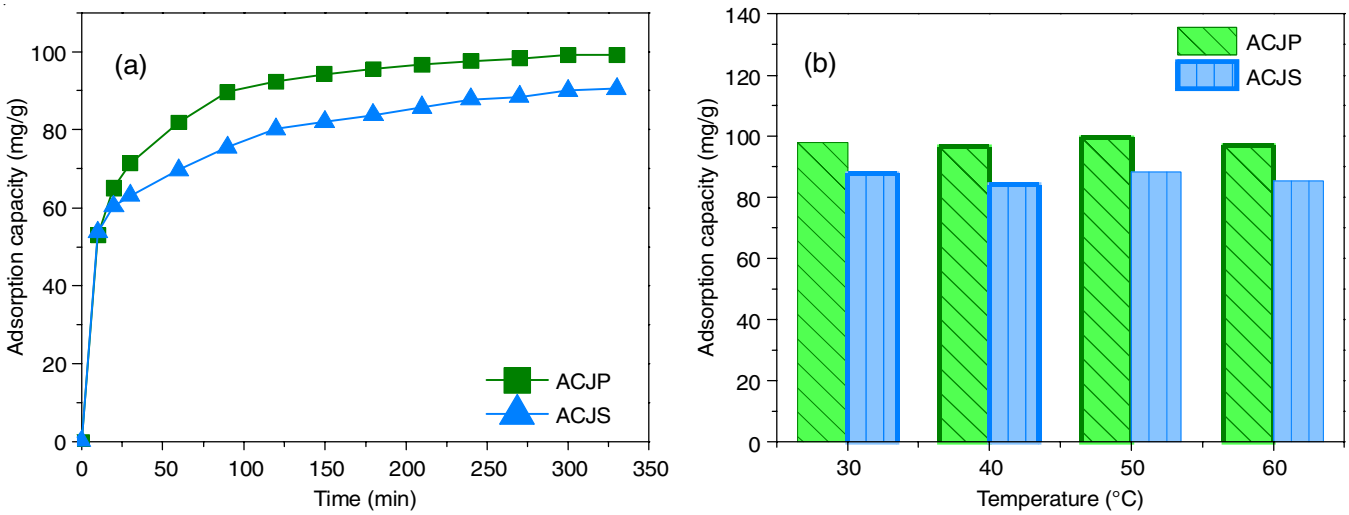

Fig. 6. Effect of time (a) and temperature (b) on the adsorption capacity of methylene blue

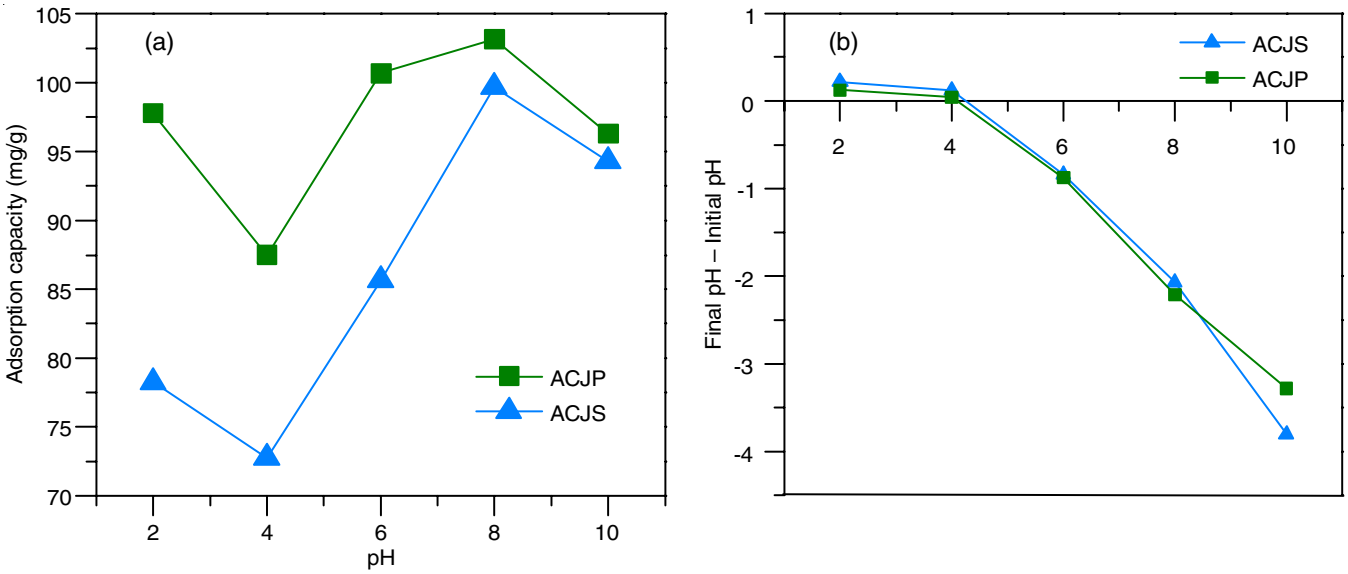

Fig. 7. Effect of solution pH (a) and The pHpzc value (b)

at pH 8 (Fig. 7b), which could be explained that the surface of the material carried a negative charge. This result was consistent with the results of FTIR analysis (with many OH^- radicals). At pH 2 and pH 4, the adsorption capacity was decreased due to the competition of free H^+ ions with S^+ of methylene blue colour molecules. At pH from 4 to 8, the decreasing H^+ ions and the increasing OH^- form favourable conditions for colour molecules to contact with the surface of the material and enter the pores [34]. Therefore, the pH 8 value was selected to evaluate other factors.

Dosage content: The adsorbent content was assessed from 0.05 to 2 g L^{-1}. When the adsorbent content was increased, the adsorption capacity decreased, thus affecting the evaluating process. It can be seen that as concentrations increased from 0.05 to 0.5 g L^{-1}, the adsorption efficiency proportionally increased from 30% to 90% (Fig. 8a-b). Then, as the content increased from 0.5 to 2 g L^{-1}, the adsorption efficiency was recorded from 90% to 100%. Specifically, at 0.5 g L^{-1}, the material was completely adsorbed the colour molecules present in the water and selected for the next factor evaluation. The methylene blue colour concentration was assessed from 0 to 200 mg L^{-1} and the adsorption process took place rapidly at the concentration from 0 to 100 mg L^{-1} and reached an almost equilibrium state at 100 mg L^{-1} (150 mg g^{-1}) (Fig. 8c). It can be seen that the concentration of 100 mg L^{-1} was the best concentration for the adsorption process. Thus, the best factors used to evaluate the kinetic and isothermal models of adsorption include time (120 min), pH (pH 8), temperature (30 ºC), dosage (0.5 g L^{-1}) and concentration (100 mg L^{-1}).

Kinetic and isothermal models: The kinetic models based on FO, PSO, Elovich and Bangham parameters were investigated and the results are shown in Fig. 9. It was found that ACJP followed the pseudo-second-order model with R^2 = 0.995, but the Elovich model with a high coefficient (R^2 = 0.992) (Table-2). Thus, the chemisorption with heterogeneous diffusion has partially occurred in the adsorption process of ACJP. For ACJS, it followed the Elovich and Bangham model with

TABLE-2
KINETIC PARAMETERS FOR THE ADSORPTION OF METHYLENE BLUE ON ACJP AND ACJS

Kinetic models	Parameters	ACJP	ACJS
PFO	q_e (mg g^{-1})	94.764	83.107
	k_1 (min^{-1})	0.059	0.070
	R^2	0.960	0.910
PSO	q_e (mg g^{-1})	101.334	88.610
	k_2 (min^{-1})	9.066	0.001
	R^2	0.995	0.969
	$H = k_2qe_2$	93095	7.852
Elovich	β (g mg^{-1})	0.076	0.091
	α (mg (g $min)^{-1}$)	93.476	127.201
	R^2	0.992	0.998
Bangham	k_B (mL L) g^{-1}	41.406	38.090
	α_B	0.158	0.151
	R^2	0.984	0.999

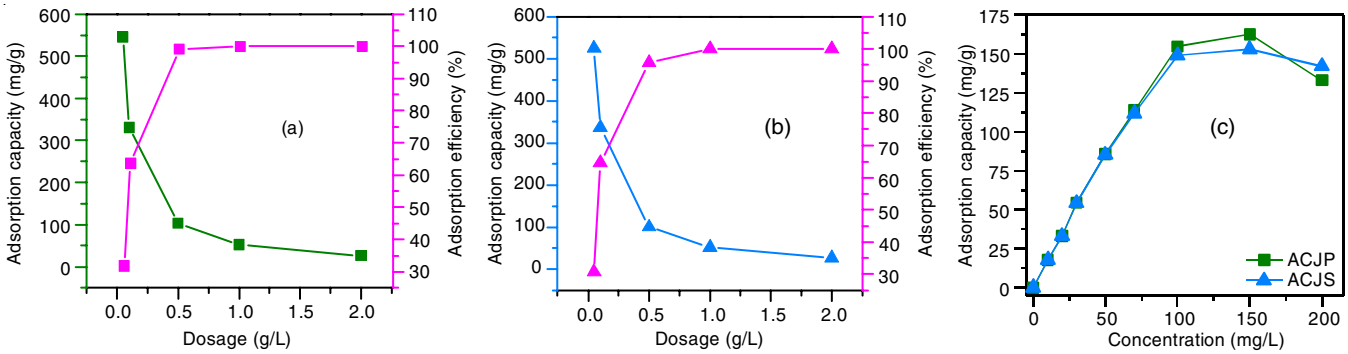

Fig. 8. Effect of adsorbent dosage from ACJP (a) and ACJS (b). Effect of dye concentration on adsorption capacity (c)

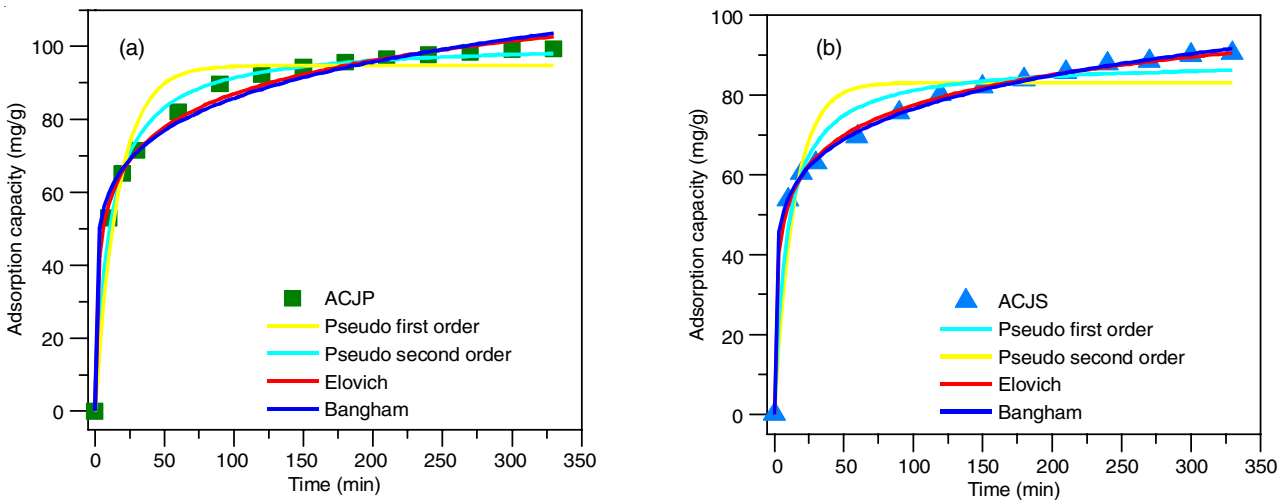

Fig. 9. Kinetic models of ACJP (a) and ACJS (b)

the coefficients R^2 = 0.998 and 0.999. It could be seen that the adsorption process of ACJS was described by adsorption with intraparticle diffusion with chemical interactions. In general, Bangham kinetic model was used to determine whether intraparticle diffusion is the predominant rate-controlling step [45]. The high correlation of Bangham kinetic model shows that pore diffusion a dominant role in methylene blue adsorption.

The adsorption process of ACJP and ACJS was evaluated by the isotherm models *viz*. Langmuir, Freundlich, Temkin, DR and the results are shown in Fig. 10. The correlation coefficient from the Langmuir model of ACJP with R^2 = 0.988 as shown in Table-3 is higher than other models. This shows that the adsorption of ACJP was represented as monolayer adsorption with uniformity of adsorption points on the surface. For ACJS, it followed the Langmuir and Temkin models with the coefficients R^2 = 0.988 and 0.983, respectively. It can be seen that the adsorption process of ACJS was described by the interaction between the adsorbent and the adsorbent on the monolayer surface and was uniform in terms of adsorption point through the process of isothermal evaluation and adsorption kinetics. The maximum adsorption capacities of ACJP and ACJS from Langmuir model were recorded at 243.316 and 230.331 mg g^{-1}. It can be seen that the adsorption process takes place with several different mechanisms including chemical interactions, multilayer adsorption and diffusion.

TABLE-3
ISOTHERMAL PARAMETERS FOR THE ADSORPTION OF METHYLENE BLUE ON ACJP AND ACJS

Isothermal models	Parameters	ACJP	ACJS
Langmuir	K_L(L mg^{-1})	0.012	0.013
	Q_m (mg g^{-1})	243.316	230.331
	R^2	0.988	0.988
	R_L	0.604	0.581
Freundlich	K_F (mg g^{-1})	9.718	10.100
	1/n	1.812	1.855
	R^2	0.957	0.952
Temkin	k_T (L/mg)	0.129	0.131
	B_T	50.946	49.608
	R^2	0.978	0.983
D-R	B (mol^2/kJ^2)	154.307	139.785
	Q_m (mg g^{-1})	152.236	147.215
	R^2	0.915	0.931
	E (kJ/mol)	0.057	0.060

Possible adsorption mechanisms: Methylene blue dye adsorbed on the activated carbon from jackfruit fruit can be by several mechanisms. As mentioned, the role of electrostatic attraction is not sufficient to explain the favourable adsorption capacity at different pH points. The FTIR results showed that the free functional groups on the surface of the material can be O-H, C=C, C-O groups. The activation of coal can generate surface oxygen and negative charge functions [46], which helps the activated carbon's ability to absorb the methylene blue acid colour slightly increase. In addition, the hydrogen interaction between the -OH group of activated carbon and the methylene blue colour molecules take place [47]. In conclusion, the plausible mechanisms of cation exchange, H-bonding and n–π interactions can shed light on methylene blue adsorption on the activated carbon from jackfruit (Fig. 11).

Response surface methodology: RSM model is built based on the values of 5 levels from the best adsorption conditions. On the basis of CCD, the relevant outcome factor was evaluated as methylene blue adsorption efficiency. A total of 20 experiments were set up from the RSM matrix (Table-4).

The quadratic equations, residual value graph, line graph and 3D between factors, analysis of variance table were analyzed and recorded. The relationship between the response coefficient (y) and the independent variables was described quadratic and determined as follows:

$$HACJP\ (\%) = 85.59 + 1.28*A - 11.92*B + 5.69*C - 4.17*AB + 0.54*AC + 2.15*BC - 1.42*A2 - 2.19*B^2 - 3{,}58*C^2$$

$$HACJS\ (\%) = 88.63 + 3.25*A - 12{,}23*B + 8.64*C + 1.2*AB + 2*AC + 3.48*BC - 3.44*A^2 - 4.14*B^2 - 1.85*C^2$$

Table-5 presented the data of analysis of variance (ANOVA) for the regression equation. The correlation coefficient (R^2), the p and F value gave expression to the significance of the

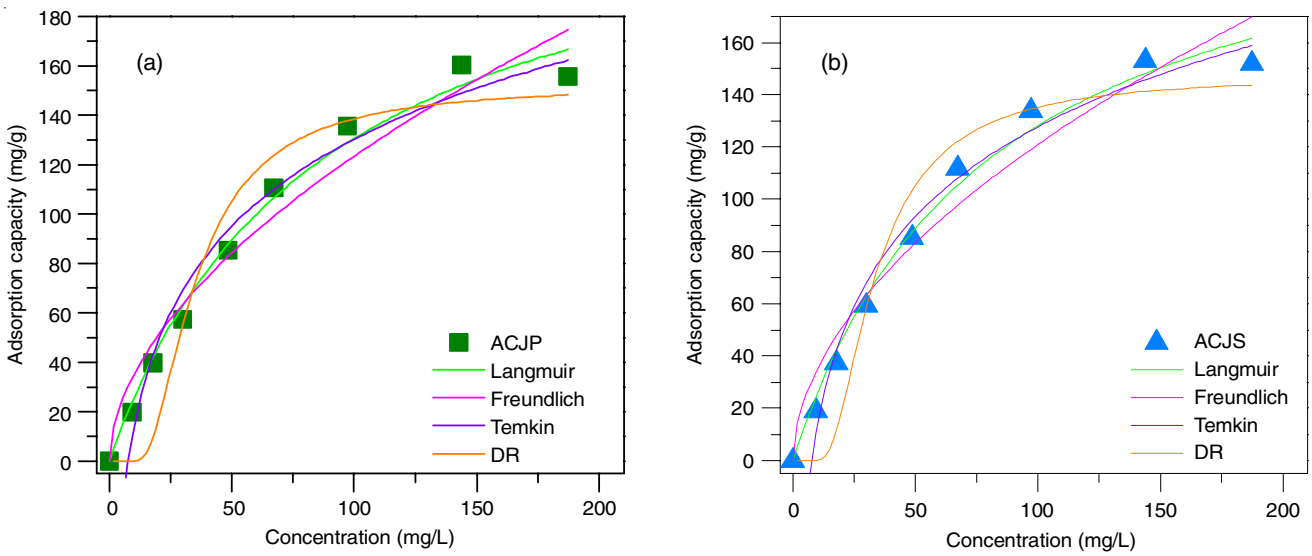

Fig. 10. Isothermal models of ACJP (a) and ACJS (b)

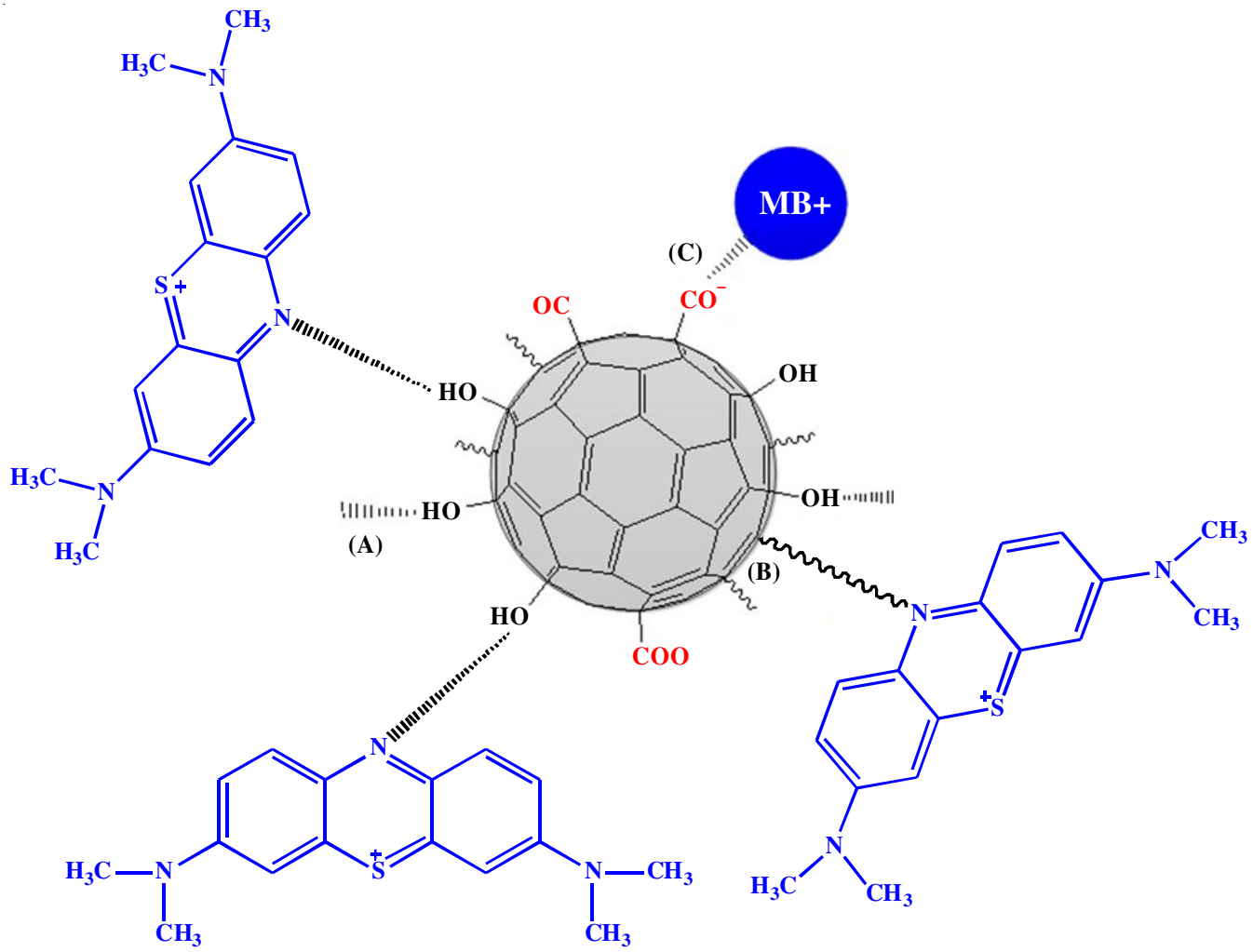

Fig. 11. Mechanism of methylene blue adsorption on activated carbon from jackfruit fruit: (a) hydrogen bonding; (b) π-π interaction; (c) electrostatic attraction

TABLE-4
EXPERIMENTAL VALUE, PREDICTION AND ERROR OF THE MODEL

Number	pH	Concentration	Content	Experimental value		Predicted value	
				ACJP	ACJS	ACJP	ACJS
1	7	50	0.4	81.86	86.00	81.87	86.22
2	9	50	0.4	92.16	86.14	91.68	86.32
3	7	100	0.4	61.94	52.20	62.07	52.40
4	9	100	0.4	55.47	57.00	55.19	57.30
5	7	50	0.6	87.54	92.00	87.86	92.54
6	9	50	0.6	99.94	100.00	99.85	100.64
7	7	100	0.6	76.16	72.00	76.68	72.66
8	9	100	0.6	71.94	84.94	71.97	85.56
9	6.32	75	0.5	80.00	74.00	79.43	73.44
10	9.68	75	0.5	83.23	85.00	83.73	84.37
11	8	32.95	0.5	99.27	98.00	99.43	97.47
12	8	117.05	0.5	59.57	57.00	59.35	56.35
13	8	75	0.33	65.50	69.00	65.88	68.87
14	8	75	0.67	85.48	99.00	85.03	97.95
15	8	75	0.5	85.53	88.50	85.59	88.63
16	8	75	0.5	85.04	88.50	85.59	88.63
17	8	75	0.5	86.36	88.73	85.59	88.63
18	8	75	0.5	85.56	90.56	85.59	88.63
19	8	75	0.5	85.07	87.97	85.59	88.63
20	8	75	0.5	85.96	87.31	85.59	88.63

TABLE-5
ANOVA VALUES OF THE RSM

Parameter	Sum of squares		Average squared		F-value		p-value	
	ACJP	ACJS	ACJP	ACJS	ACJP	ACJS	ACJP	ACJS
Model	2829.18	3746.78	314.35	416.31	1043.96	408.10	< 0.0001	< 0.0001
A-pH	22.26	144.22	22.26	144.22	73.93	141.38	< 0.0001	< 0.0001
B-concentration	1939.74	2040.99	1939.74	2040.99	6441.80	2000.76	< 0.0001	< 0.0001
C-dosage	442.66	1020.49	442.66	1020.49	1470.08	1000.38	< 0.0001	< 0.0001
AB	139.36	11.52	139.36	11.52	462.82	11.29	< 0.0001	0.0072
AC	2.37	32.00	2.37	32.00	7.86	31.37	0.0187	0.0002
BC	37.11	97.16	37.11	97.16	123.24	95.25	< 0.0001	< 0.0001
A^2	28.92	170.19	28.92	170.19	96.04	166.84	< 0.0001	< 0.0001
B^2	69.23	247.44	69.23	247.44	229.90	242.56	< 0.0001	< 0.0001
C^2	184.86	49.08	184.86	49.08	613.91	48.12	< 0.0001	< 0.0001

regression models. In general, the model is statistically significant, since the smaller the p-value and the larger the F-value. The p value when greater than 0.05, the model is effective (expressing the statistical significance of the influencing factors with 95% confidence) and *vice-versa* when it is less than 0.05. The results of ANOVA analysis showed that the predictive value model was compatible with the experimental value and had statistical significance ($p < 0.05$). The correlation coefficients of ACJP and ACJS materials were 0.999 and 0.997 > 0.75, respectively.

The normal probability plot, the residual *versus* predicted value plot and the actual *versus* predicted value plot are shown in Fig. 12. The points lie approximately on a straight line in Fig. 12a,d, representing the normal distribution of the residuals. In Fig. 12b,e, it is shown that the points are clustered near the diagonal, showing a good correlation between the experimental and predicted values. Fig. 12c,f, the distribution of these points is random and the position is within ±4.0, which confirms the appropriateness of the experimental model [48,49]. The linearity of the normal probability plot for the residuals shows the accuracy of the proposed model. The remaining values are randomly distributed over the number of runs indicating the accuracy of the model.

Experimental conditions such as colorant concentration (mg L^{-1}), amount of ACJP or ACJS adsorbent (g L^{-1}) and pH value were optimized by RSM model. As shown in Fig. 13, the

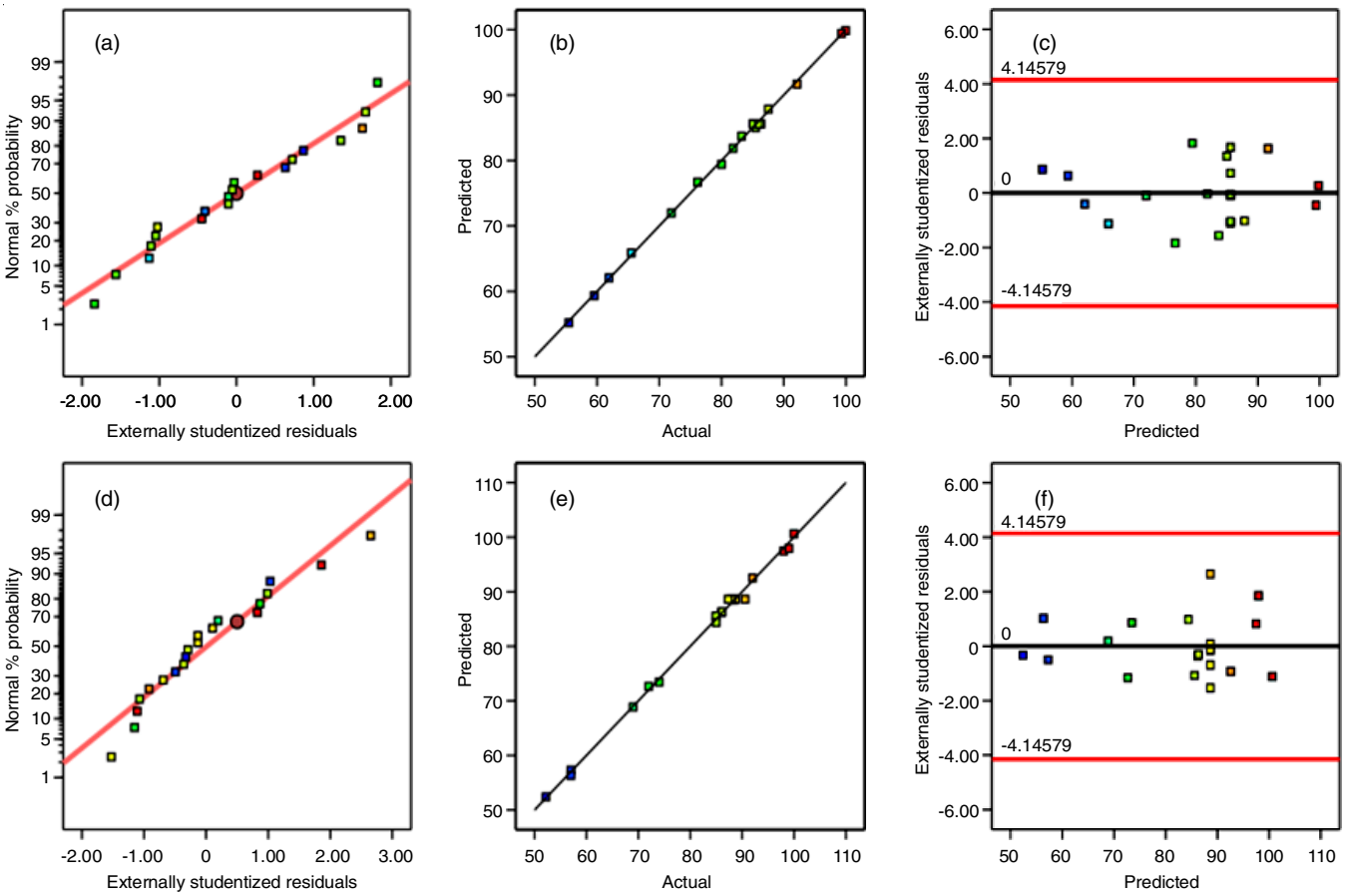

Fig. 12. Residual plots of ACJP and ACJS as (a,d) normal plot of residuals, (b,e) the actual and predicted values, (c,f) residual *vs*. predicted

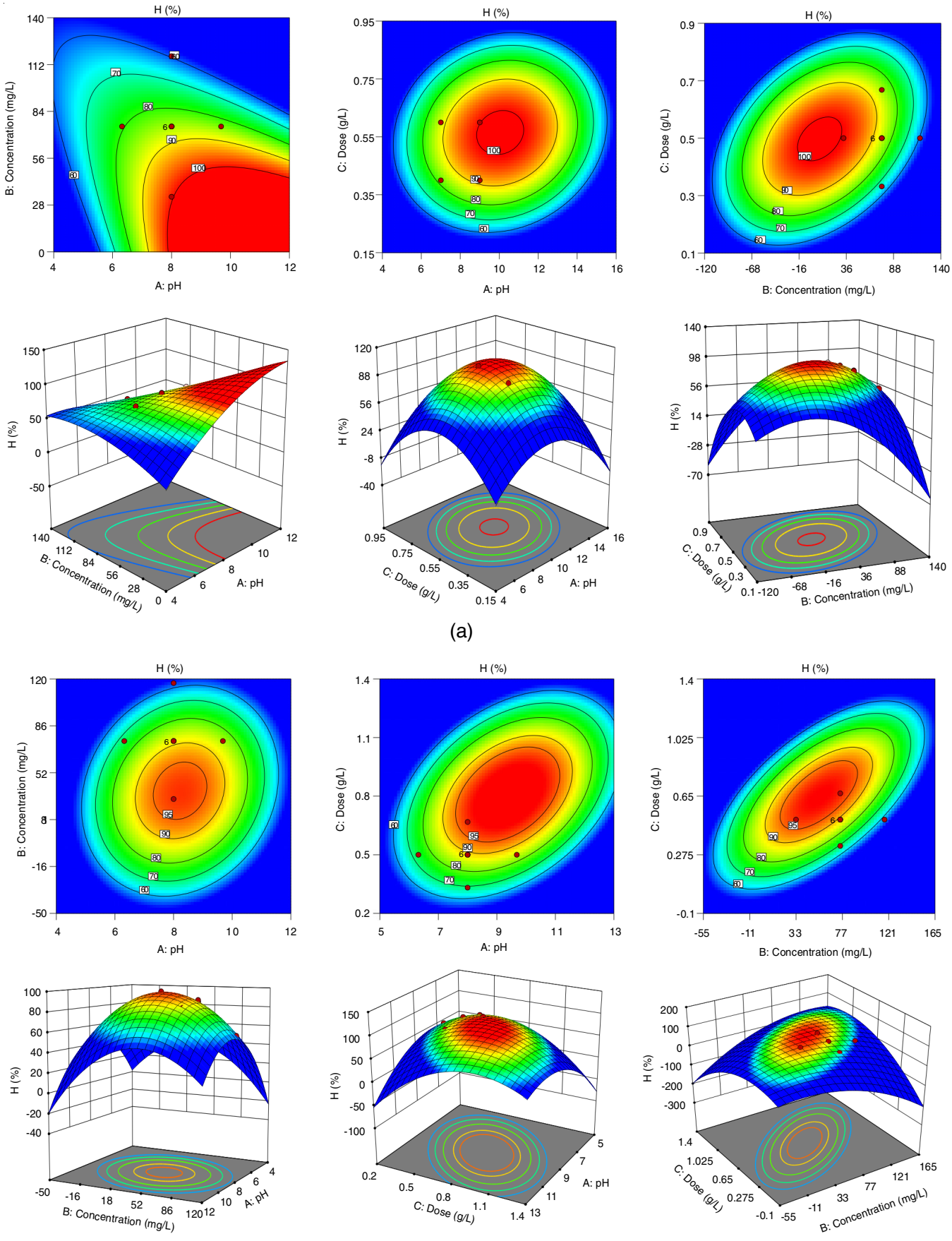

Fig. 13. Line diagram and surface plot of ACJP (a) and ACJS (b)

surface response plot can also see the high value region of the model to capture the optimal value of the material. ACJP was recorded to have a pH convergence point greater than pH 8, concentrations from 0 mg L^{-1} to 50 mg L^{-1} and concentrations less than 0.5 g L^{-1}. For ACJS materials with convergence point with pH value in the range of pH 8 to pH 10, the concentration is about 20 mg L^{-1} to 60 mg L^{-1} and the concentration ranges from 0.6 g L^{-1} to 1 g L^{-1}. The surface histogram and the 3D model both show the optimal region from the evaluation model and show the interaction between the elements through the optimal region.

The optimal area of the influencing factors was calculated and selected the optimal values. The optimal values of ACJP and ACJS materials are clearly matched with the most optimal values (Fig. 14). The value of ACJP materials was recorded at pH 8.97, concentration of 50.5 mg L^{-1} and content of 0.57 g L^{-1}. The adsorption capacity and efficiency from the RSM prediction is 90.82 mg g^{-1} with 100% under the optimal conditions. For ACJS materials, the optimum value was recorded at pH 8.61, concentration 52 mg L^{-1} and dosage 0.57 g L^{-1}. Ths, the adsorption capacity and efficiency from the RSM model prediction is 94.04 mg g^{-1} with 100% under the optimal conditions. From the optimal results, the ACJS and ACJP gives the same maximum adsorption capacity.

Reusability study: Using the optimized conditions *viz.* time (120 min), pH (pH 8), temperature (30 ºC), content (0.5 g L^{-1}) and concentration (100 mg L^{-1}), the reusability of both adsorbents was investigated. Alcohol solvent was used to remove methylene blue inside the material and the washing process was repeated 3 times to remove the methylene blue. The raw materials after removing colourants had been dried at 100 ºC for 24 h. The material was then taken for the next reuse assessment and the results have shown that ACJS and ACJP material can be re-used atleast for three times (Fig. 15). The adsorption efficiency was half as good after the third reuse, suggesting the material has been losing its capacity to release dye molecules into the environment.

Cost analysis: The economic evaluation of a production system can provide an overview of the system's potential economic profits [50]. In particular, the assessment is applied to several interdependent stages, *i.e.* raw material cost (RMC), transportation cost (TC) and handling cost (PC) [51]. Thus, the estimated costs for activated carbon production were calculated as total direct operating costs (TTC) including raw material costs (RM) and chemicals costs (CH). Raw materials from local waste treatment sites cost 0.20 $/kg fresh ingredients = 0.49$/kg dry powder. Chemicals used including NaOH and HCl cost 2.16 $/bottle. The production process requires 2 bottles of NaOH and 1 bottle of HCl. Total cost of chemicals is 6.47 $/3 bottles, which are represented in the following equation: TTC = RM + CH. Total direct operating cost is 7.48$ for 2.5 kg of skin or pulp, which become approximately 3 $/kg. The activated carbon

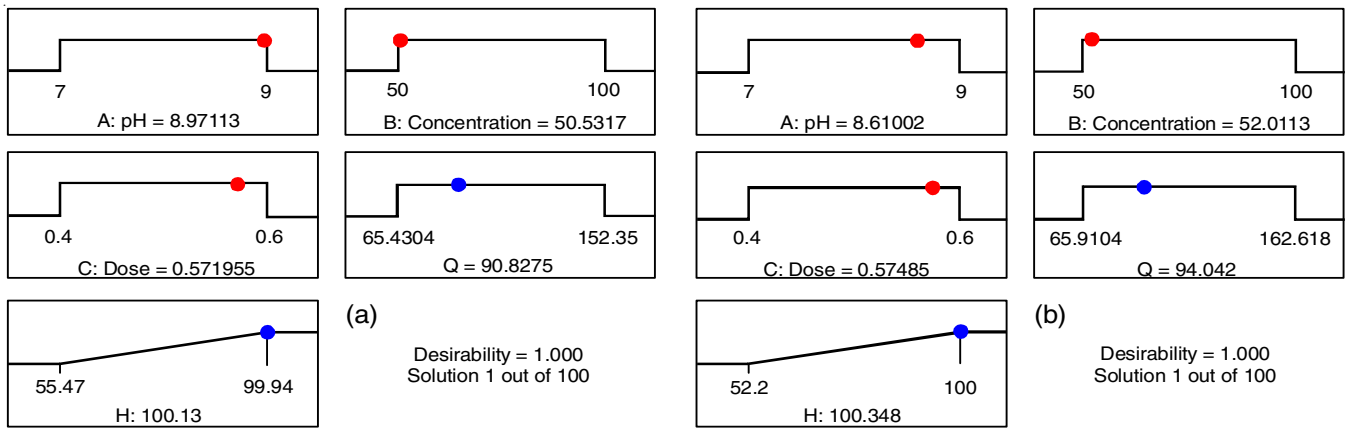

Fig. 14. Optimal values from the model of ACJP (a) and ACJS (b)

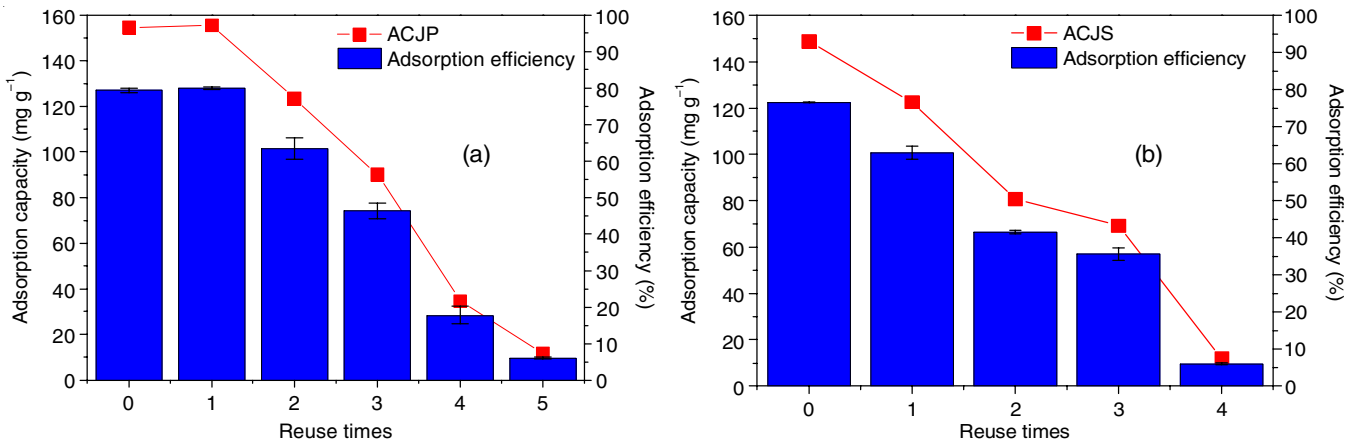

Fig. 15. The reusability of ACJP (a) and ACJS (b)

prices from the Chinese market range from 1.8 to 5.2 USD/kg, therefore, the estimated product cost is still within the market price range.

Conclusion

Activated carbon was synthesized by microwave-assisted method. The structural and physical properties were analyzed by SEM, XRD, FTIR, BET analysis. The surface area and pore volume have been improved as compared to the raw material. With the characteristic semi-crystalline structure and functional groups, the adsorption capacity has been evaluated in the most specific way. The adsorption process shows that ACJP follows the model of pseudo-second-order (PSO) and Langmuir, while ACJS follows the Bangham model and Langmuir isotherm. It can be seen that the adsorption process takes place with many different mechanisms including chemical interactions, multi-layer adsorption and diffusion. The parameters for the adsorption process were also optimized from the RSM model with ACJP (pH 8.97, concentration of 50.5 mg L^{-1} and dosage of 0.57 g L^{-1}, with adsorption capacity 90.82 mg g^{-1}, 100% efficiency) and ACJS (pH 8.61, concentration 52 mg L^{-1} and dosage of 0.57 g L^{-1}, with adsorption capacity 94.04 mg g^{-1}, 100% efficiency), respectively. The both derived activated materials also shows a long-term application potential as the reusability was recorded as three times.

ACKNOWLEDGEMENTS

The study was supported by The Youth Incubator for Science and Technology Programmed, managed by Youth Development Science and Technology Center, Ho Chi Minh Communist Youth Union and Department of Science and Technology of Ho Chi Minh City (contract no. 40/2021/HĐ-KHCNT-VU signed on 8th, December 2021).

CONFLICT OF INTEREST

The authors declare that there is no conflict of interests regarding the publication of this article.

REFERENCES

1. A.U. Khan, I.J. Ema, M.R. Faruk, S.A. Tarapder, A.U. Khan, S. Noreen and M. Adnan, *J. Multidiscip. Appl. Nat. Sci.*, **1**, 106 (2021); https://doi.org/10.47352/jmans.v1i2.88
2. A. Witt and Q. Luke, Guide to the Naturalized and Invasive Plants of Eastern Africa, UK: CABI (2017).
3. J.R. Rajabathar, S. Manoharan, J.V. J, H.A. Al-Lohedan and P. Arunachalam, *J. Energy Storage*, **32**, 101735 (2020); https://doi.org/10.1016/j.est.2020.101735
4. M.S. Baliga, A.R. Shivashankara, R. Haniadka, J. Dsouza and H.P. Bhat, *Food Res. Int.*, **44**, 1800 (2011); https://doi.org/10.1016/j.foodres.2011.02.035
5. O. Prakash, R. Kumar, A. Mishra and R. Gupta, *Pharmacogn. Rev.*, **3**, 353 (2009).
6. V. Shinde, C.D. Pawar, O.S. Warang, V.S. Dandekar, M.M. Kulkarni, J. J and M.S. Joshi, *Int. J. Chem. Stud.*, **9**, 2710 (2021); https://doi.org/10.22271/chemi.2021.v9.i1al.11636
7. S. Meethal, N. Kaur, J. Singh and Y. Gat, *Curr. Res. Nutr. Food Sci.*, **5**, 154 (2017); https://doi.org/10.12944/CRNFSJ.5.2.12
8. K. Das and A. Saha, *J. Medicinal Plants Studies*, **8**, 101 (2020); https://doi.org/10.33545/26631067.2020.v2.i2a.42
9. R. Felli, T.A. Yang, W.N. Wan Abdullah and W. Zzaman, *Trop. Life Sci. Res.*, **29**, 113 (2018); https://doi.org/10.21315/tlsr2018.29.1.8
10. M. Rengasamy, R.V. Raj and N. Vedagiriswaran, *Elixir Renewable Energy*, **102**, 44269 (2017).
11. R. Shamsudin, C.S. Ling, C.N. Ling, N. Muda and O. Hassan, *J. Appl. Sci.*, **9**, 3202 (2009); https://doi.org/10.3923/jas.2009.3202.3204
12. A.A. Sundarraj and T.V. Ranganathan, *Int. J. Pharm. Sci. Res.*, **9**, 1000 (2018).
13. K. Subburamu, M. Singaravelu, A. Nazar and I. Irulappan, *Bioresour. Technol.*, **40**, 85 (1992); https://doi.org/10.1016/0960-8524(92)90125-H
14. M. Duque-Acevedo, L.J. Belmonte-Ureña, F.J. Cortés-García and F. Camacho-Ferre, *Glob. Ecol. Conserv.*, **22**, e00902 (2020); https://doi.org/10.1016/j.gecco.2020.e00902
15. K.N.T. Tran, B.N. Hoang, K.O.T. Nguyen, H.T.T. Nguyen, S.C. Phung, H.T. Do and C.Q.T. Ngo, *Indonesian J. Chem.*, **22**, 565 (2021); https://doi.org/10.22146/ijc.69538
16. M.F. Abbod, J.W.F. Catto, D.A. Linkens and F.C. Hamdy, *J. Urol.*, **178**, 1150 (2007); https://doi.org/10.1016/j.juro.2007.05.122
17. N. Abbas, M. Hussain, N. Russo and G. Saracco, *Chem. Eng. J.*, **175**, 330 (2011); https://doi.org/10.1016/j.cej.2011.09.115
18. M. Ashokkumar and P. Arunachalam, *Appl. Catal. A Gen.*, **555**, 47 (2018); https://doi.org/10.1016/j.apcata.2018.02.010
19. H. Guan, H. Wang, Y. Zhang, C. Dong, G. Chen, Y. Wang and J. Xie, *Appl. Surf. Sci.*, **447**, 261 (2018); https://doi.org/10.1016/j.apsusc.2018.03.225
20. A. Nayak, B. Bhushan, V. Gupta and S. Kotnala, *J. Ind. Eng. Chem.*, **100**, 134 (2021); https://doi.org/10.1016/j.jiec.2021.05.028
21. D. Prahas, Y. Kartika, N. Indraswati and S. Ismadji, *Chem. Eng. J.*, **140**, 32 (2008); https://doi.org/10.1016/j.cej.2007.08.032
22. R. Gokulan, G.G. Prabhu and J. Jegan, *Int. J. Phytoremediation*, **21**, 1179 (2019); https://doi.org/10.1080/15226514.2019.1612845
23. M.F. Mohamad Yusop, A.Z. Abdullah and M.A. Ahmad, *Diamond Rel. Mater.*, **136**, 109991 (2023); https://doi.org/10.1016/j.diamond.2023.109991
24. V. Parimelazhagan, K. Natarajan, S. Shanbhag, S. Madivada and H.S. Kumar, *Chem. Eng.*, **7**, 31 (2023); https://doi.org/10.3390/chemengineering7020031
25. P. Vairavel, N. Rampal and G. Jeppu, *Int. J. Environ. Anal. Chem.*, **103**, 2789 (2023); https://doi.org/10.1080/03067319.2021.1897982
26. V. Parimelazhagan, P. Yashwath, D.A. Pushparajan and J. Carpenter, *Int. J. Mol. Sci.*, **23**, 12484 (2022); https://doi.org/10.3390/ijms232012484
27. V. Chandanshive, S. Kadam, N. Rane, B.-H. Jeon, J. Jadhav and S. Govindwar, *Chemosphere*, **252**, 126513 (2020); https://doi.org/10.1016/j.chemosphere.2020.126513
28. M.F. Mohamad Yusop, M.N. Nasehir Khan, R. Zakaria, A.Z. Abdullah and M.A. Ahmad, *Arab. J. Chem.*, **16**, 104780 (2023); https://doi.org/10.1016/j.arabjc.2023.104780
29. H. Li, L. Liu, J. Cui, J. Cui, F. Wang and F. Zhang, *RSC Adv.*, **10**, 14262 (2020); https://doi.org/10.1039/D0RA01245A
30. I. Khan, K. Saeed, I. Zekker, B. Zhang, A.H. Hendi, A. Ahmad, S. Ahmad, N. Zada, H. Ahmad, L.A. Shah, T. Shah and I. Khan, *Water*, **14**, 242 (2022); https://doi.org/10.3390/w14020242
31. M.T. Yagub, T.K. Sen, S. Afroze and H.M. Ang, *Adv. Colloid Interface Sci.*, **209**, 172 (2014); https://doi.org/10.1016/j.cis.2014.04.002
32. A. Asfaram, M. Ghaedi, S. Hajati, M. Rezaeinejad, A. Goudarzi and M.K. Purkait, *J. Taiwan Inst. Chem. Eng.*, **53**, 80 (2015); https://doi.org/10.1016/j.jtice.2015.02.026

33. E. Altintig, H. Altundag, M. Tuzen and A. Sari, *Chem. Eng. Res. Des.*, **122**, 151 (2017); https://doi.org/10.1016/j.cherd.2017.03.035
34. M. Das and C. Mishra, *SN Appl. Sci.*, **1**, 483 (2019); https://doi.org/10.1007/s42452-019-0459-7
35. K.Y. Foo and B.H. Hameed, *Bioresour. Technol.*, **112**, 143 (2012); https://doi.org/10.1016/j.biortech.2012.01.178
36. N.T.C. Quyen, T.L. Van, L.G. Bach and B.N. Hoang, *Key Eng. Mater.*, **949**, 175 (2023); https://doi.org/10.4028/p-VfN0Z5
37. B.N. Hoang, T.T. Nguyen, Q.P.T. Bui, L.G. Bach, D.-V.N. Vo, C.D. Trinh, X.-T. Bui and T.D. Nguyen, *J. Appl. Polym. Sci.*, **137**, 48904 (2020); https://doi.org/10.1002/app.48904
38. N.H. Bich, T.N. Thuong, V.N. Dai and V.T. Lam, *Mater. Today Proc.*, **38**, 3046 (2021); https://doi.org/10.1016/j.matpr.2020.09.391
39. T.T. Nguyen, B.N. Hoang, T.V. Tran, D.V. Nguyen, T.D. Nguyen and D.-V.N. Vo, *Surf. Interfaces*, **26**, 101410 (2021); https://doi.org/10.1016/j.surfin.2021.101410
40. P. Vairavel and V. Ramachandra Murty, *Desalination Water Treat.*, **103**, 84 (2018); https://doi.org/10.5004/dwt.2018.21799
41. X. Ge, Z. Wu, Z. Wu, Y. Yan, G. Cravotto and B.-C. Ye, *J. Ind. Eng. Chem.*, **39**, 27 (2016); https://doi.org/10.1016/j.jiec.2016.05.003
42. M.Z. Hossain, W. Wu, W.Z. Xu, M.B.I. Chowdhury, A.K. Jhawar, D. Machin and P.A. Charpentier, *C*, **4**, 38 (2018); https://doi.org/10.3390/c4030038
43. B. Bhushan, A. Nayak and S. Kotnala, *Mater. Today Proc.*, **44**, 187 (2021); https://doi.org/10.1016/j.matpr.2020.08.554
44. L. Ramasamy and L.R. Miranda, *Adsorpt. Sci. Technol.*, **2022**, 4129833 (2022); https://doi.org/10.1155/2022/4129833
45. L. Xie, Y. Meng, Q. Wang, G. Zhang, H. Xie and G. Zhou, *Diamond Rel. Mater.*, **130**, 109474 (2022); https://doi.org/10.1016/j.diamond.2022.109474
46. X. Zhang, Y. Wang, J. Cai, K. Wilson and A.F. Lee, *Energy Environ. Mater.*, **3**, 453 (2020); https://doi.org/10.1002/eem2.12074
47. Y. Zhu, B. Yi, Q. Yuan, Y. Wu, M. Wang and S. Yan, *RSC Adv.*, **8**, 19917 (2018); https://doi.org/10.1039/C8RA03018A
48. H. Dadkhah and M.A. Behnajady, *Chem. Eng. Commun.*, **206**, 398 (2019); https://doi.org/10.1080/00986445.2018.1494581
49. X. Ma, S. Tian, X. Li, H. Fan and S. Fu, *Cellulose*, **28**, 8027 (2021); https://doi.org/10.1007/s10570-021-03989-2
50. A.C. Fingolo, B.C. Klein, M.C.A.F. Rezende, C.A. Silva e Souza, J. Yuan, G. Yin, A. Bonomi, D.S.T. Martinez and M. Strauss, *Waste Biomass Valoriz.*, **11**, 1 (2020); https://doi.org/10.1007/s12649-019-00774-y
51. C.D. Sulistiyo, K.-C. Cheng, H.J. Su'andi, M. Yuliana, C.-W. Hsieh, S. Ismadji, A.E. Angkawijaya, A.W. Go, H.Y. Hsu, P.L. Tran-Nguyen and S.P. Santoso, *J. Clean. Prod.*, **380**, 135010 (2022); https://doi.org/10.1016/j.jclepro.2022.135010